

Article

A Low-Cost Platform for Modeling and Controlling the Yaw Dynamics of an Agricultural Tractor to Gain Autonomy

Sergio Sandoval Pérez ¹, Juan Miguel González López ^{2,*}, Ramón O. Jimenez Betancourt ²,
Efraín Villalvazo Laureano ², Jesús Ezequiel Molinar Solís ¹,
María Guadalupe Sánchez Cervantes ¹ and Víctor Javier Ochoa Guzmán ¹

¹ Tecnológico Nacional de México/Instituto Tecnológico de Ciudad Guzmán, Ciudad Guzmán 49100, Mexico; ssandoval@itcg.edu.mx (S.S.P.); jemolinars@itcg.edu.mx (J.E.M.S.); msanchez@itcg.edu.mx (M.G.S.C.); victor11290383@itcg.edu.mx (V.J.O.G.)

² Facultad de Ingeniería Electromecánica, Universidad de Colima, Manzanillo 28860, Mexico; rjimenez@uacol.mx (R.O.J.B.); villalvazo@uacol.mx (E.V.L.)

* Correspondence: jgonzalez71@uacol.mx

Received: 28 September 2020; Accepted: 30 October 2020; Published: 2 November 2020



Abstract: In this study, a low-cost proposed platform for training dynamics (PPTD) is proposed based on operational amplifiers to understand the dynamics and variables of the agricultural tractor John Deere tractor model 4430 to gain autonomy and analyze the behavior of control algorithms proposed in real time by state feedback. The proposed platform uses commercial sensors and interacts with the Arduino Uno and/or Daq-6009 board from National Instruments. A mobile application (APP) was also developed for real-time monitoring of autonomous control signals, the local reference system, and physical and dynamic variables in the tractor; this platform can be used as a mobile alternative applied to a tractor in physically installed form. In the presented case, the PPTD was mounted on a John Deere tractor to test its behavior; moreover, it may be used on other tractor models similarly as established here. The established results of this platform were compared with models established in MATLAB, validating the proposal. All simulations and developments are shared through a web-link as open-source files so that anyone with basic knowledge of electronics and modeling of vehicles can reproduce the proposed platform.

Keywords: vehicle dynamics models; autonomous agricultural vehicles; hardware platform framework

1. Introduction

The use of vehicles with diverse technologies such as mechanical, hybrid, or electrical machines operated for different activities in transportation and industrial application, amount others, requires safety and more efficient behavior; these needs motivate the research in the design of new electronic devices for car control and driver-assisted systems, such as in [1] where a methodology is proposed based on single-input single-output yaw controller ensuring rapid control action in critical situations, such as the case of oversteering of the vehicle. These controllers modify vehicle dynamics by imposing forces or moments in different actuators with the help of sensors that allow precise measurements, providing high efficiency in the performance of actions and contributing to vehicle stability, safety, and comfort [2–7]. In agriculture, tractors are one of the important tools for humans, contributing to the food generation and cultivation techniques. For instance, Ref. [8] describes the development of a novel wheel robotic in the production process utilizing solar panels to execute monitoring tasks. Actually, there is an increasing interest in autonomous vehicle systems considering

kinematic and dynamic behavior [9]; such interest also extends agricultural vehicles in different labors in agribusiness [10–14].

The aspects of security and stability have been considered in the literature, with a focus on analyzing their performance. The work of [15] established virtual reality (VR) experiments to test different working conditions of the wheel with the terrain. In [16], experiments were conducted on the tractor autonomy of the branch New Holland TZ25DA model with the help of LabVIEW and PXI system in modeling the dynamics and implementing a frequency domain identification method to determine the tire side-slip angles and lateral forces. In [17], a platform was developed for traffic safety operation with a 2 degree of freedom driving simulator. In [18], the authors proposed a test simulator to analyze the stability considering the angles on the bench roll through a physical platform cab. The authors of [16] carried out the modeling simulation of an agricultural vehicle with a rollover protection structure, determining that some dynamics may affect a collision when hitting on a slope by using friction coefficient data for dry conditions and with flooded detergent. In [19,20], discussions are presented regarding the state of the art in autonomous driving vehicles focused on the top 20 countries in the world, dividing the autonomy into six levels based on the difficulty to be handled in the design of driverless vehicles, including different technologies equipped such as sensing, positioning, vision, and vehicular networks. Another survey is presented in [21], focusing on deep learning methods for autonomous vehicle control.

Commercial software such as CarSim, TruckSim, and BikeSim, and ADAMS Car is utilized for educational and analysis. In [22], simulation techniques are used to teach vehicle theory and design with the help of ADAMS/car and MATLAB/Simulink. The authors of [23] analyzed the mathematical model of a mobile robot with wheels called Tractor-Trailer, analyzing the longitudinal and lateral sliding of the tires, in addition to the proposal of robust dynamic control based on a sliding mode algorithm to solve the problem in MATLAB/Simulink–CarSim and implement a real-time laboratory platform for an electric vehicle. The authors of [24] modeled a light electric vehicle using PSIM to improve student skills on the powertrain. Nevertheless, most of them assume that the mathematical understanding of the model has been acquired and focus only on the analysis, modeling, and design of controllers without considering the need to generate experience in the design and testing of a physical controller.

There are some other learning platforms in the commercial area, such as that of D’Lorenzo [25], for understanding the systems in the vehicles, but each learning kit has a cost of about USD 10,000, without considering that they have no platform for the study of the tractor. Another strategy could be the use of platforms such as the case of hardware-in-the-loop, but this also comes at a high cost [26]. Similarly, there is commercial equipment applied to agricultural vehicles with differential global positioning systems (DGPSs), such that developed by New Holland company through the system called EZ-Guide that consists of a high-definition screen based on GPS controlling the tractor autonomy utilizing an EZ-Steer actuator, which uses real-time kinematic navigation, allowing the operation to be managed from a computer, tablet, or cellphone in real time [27]. On the other hand, John Deere considers autonomy in the semi-autonomous electric tractor with its See & Spray technology with satellite technology based on artificial intelligence incorporating a joystick control, touch screen, and the integration of all components in the machine [28]. However, there is still a high cost in the implementation of high-precision technology. Therefore, due to the economic problems around the world, several institutions have begun developing prototypes to meet the need for low-cost equipment in their laboratories [29].

Mexico is facing problems related to a reduction in food production due to climate change [30]. Furthermore, inequality in the Mexican agrarian structure limits the ability of farmers to update technology to increase their production [31]. One of the strategies that help increase production would be the automation of processes in crop production with their existing equipment, such as the tractor. Thus, as a first step, the implementation of a prototype hardware–software including the basics may

offer a simple means to design a physical controller and better understand the tractor dynamics with the aim of low-cost underlying components and processes.

Considering the above information, a low-cost platform is proposed in this work considering the international ISO 7401/2011 standard with the design of electronic boards, including measurements and physical parameter estimations applied to the tractor dynamics. The strengths of the proposed platform are its simplicity of reproduction since it is based on operational amplifier circuits, which can be acquired easily at a low cost. Furthermore, the mathematical model is described in detail, as is its implementation in Proteus software using a farm vehicle established as a rigid body, and shared as an open-source file. Thus, an electronic circuit board is designed to be implemented physically on a tractor and obtain the main variables. The physical application of the proposed platform was tested on a John Deere tractor, model 4430, through an electric assistance actuator (electric motor) coupled to the steering wheel to obtain vehicle autonomy. Additionally, the platform also considers the utilization of an application (APP) that displays the main variables in real time on a cellphone or tablet screen. Validation was conducted considering models found in the literature and programmed in Simulink. Moreover, open-source simulations and electronic board designs are shared with the community and are able to be reproduced as part of the contribution of the present work.

2. System Description and Modeling

2.1. System Configuration

Figure 1 depicts a block diagram of the proposed system to demonstrate dynamics and understanding of the variables that affect vehicle autonomy; each fragment is described in the following sections.

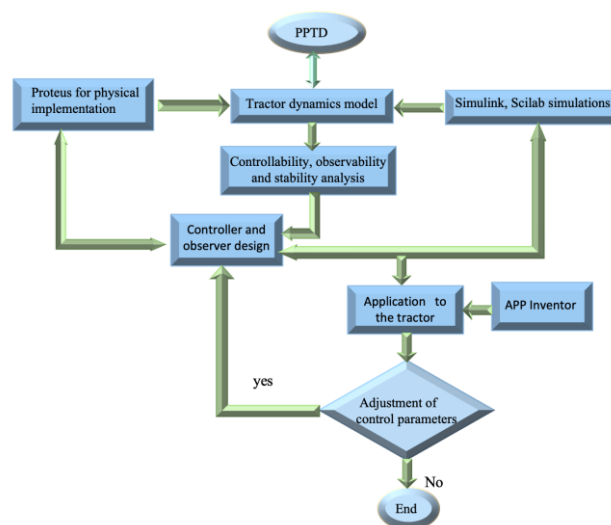


Figure 1. Platform operation logic function.

The module of Figure 1 is implemented by RF or Bluetooth (with the proposed APP control) activation of the direct current motor (M) working as an actuator coupled to the steering wheel system, in this case, that of the John Deere tractor, thereby driving the front wheel turning angles. The sequence is shown in Figure 2. The ignition power cuts and the activation of the electric actuator (M) use a 12-V 30–40 A five-pin Ford-type relay. An inverter with characteristics of 12 V dc to 110 V ac of 1500 W (to be implemented in the real tractor) is connected to a dual source of +12 V/−12 V/3 A, feeding the proposed platform for training dynamics (PPTD) which receives the measurements from the signal conditioner with inputs a, b, coming from the electric motor terminals (M); this generates the input signals, such as the wheel angle δ , $-\delta$ (with international standard ISO 7401/2011, where $\delta = \delta_d + \delta_c$, δ_d : proximity sensor signal, δ_c : control signal, δ , $-\delta$: turning signal to right/left) to the PPTD, producing

the dynamics and vehicle variables that are sent to a low-cost Arduino card or a DAQ 6009 where the autonomous control algorithms connected to relays of 5 V at 10 A and 12 V at 30 or 40 A are programmed, activating the electric actuator (M), which performs the autonomy task.

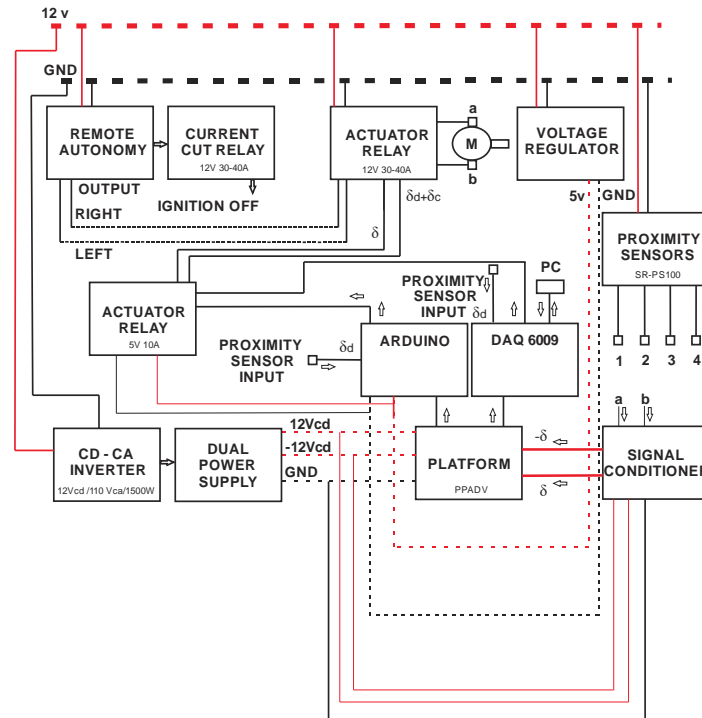


Figure 2. Overview of the proposed platform for training dynamics (PPTD) to analyze vehicle dynamics and variables.

2.2. Tractor Dynamic Tire Models

The mathematical model for a farm vehicle can be established as a rigid body moving in free space of two or three degrees of freedom connected to a flat land surface through the tires (Figure 3). Besides, when considering the estimation of linear and nonlinear dynamics, these can be analyzed in a simplified way with the so-called bicycle model [32,33], resulting in being able to propose a measurement of the variable δ_d :

$$m(\dot{v}_x - v_y\omega_z) = ma_x \tag{1}$$

$$m(\dot{v}_y + v_x\omega_z) = [F_{f,y}(\delta_c + \delta_d, x, \alpha_f) + F_{r,y}(x, \alpha_r)] \tag{2}$$

$$J\dot{\omega}_z = [l_f F_{f,y}(\delta_c + \delta_d, x, \alpha_f) - l_r F_{r,y}(x, \alpha_r)] + M_z \tag{3}$$

where m is the vehicle mass (kg); J is the moment of inertia (kg m^2); l_f, l_r are lengths (m) from the center to the front and rear, respectively; v_x, v_y are the longitudinal and lateral velocity (m/s), $\beta = \tan^{-1}(v_y/v_x)$, chassis side slide (rad); $x = (v_y, v_x)$ is the compact state vector; $\omega_z \cong \dot{\delta}_{dact}R$ is the angular velocity of turn (rad/s), which is in synchrony with δ_d [34,35], considering $\omega_z \neq 0$, with $\omega_{zmin} \leq |\omega_z| > 0$, with a minimum value of (ω_{zmin}) , for a time $t \geq 0$ s when the sensor SR-PS100 does not detect δ_d , and $R > 0$ is a constant gain which is chosen so that the angular velocity of the turn is not saturated, which relates the input voltage on the actuator with the angular velocity which is obtained from [36]; α_f, α_r are front and rear side slip angles (rad); δ_d, δ_c are the tire angle components imposed by the driver and controller (rad); $\dot{\delta}_{dact} = (u_m - R_m I)/k_b$ is the angular velocity response of the actuator on the tractor steering wheel (rad/s) and is established as +DDELTA 1 VOL and +DDELTA 2 VOL on the PPTD shown in Appendix A, where u_m is the input voltage to actuator (V), $k_b > 0$ is an estimated back electromotive force constant (V/(rad/s)), R_m is the resistance of the actuator (Ω), and I is the current

(A), considering the simplified mathematical model of the cc motor where its values are obtained experimentally; M_z the moment of turn resulting from the active brakes (N m); lateral forces $F_{f,y}$, $F_{r,y}$ (N) are functions of the angle imposed on the front tires ($\delta = \delta_d + \delta_c$), where δ_d and δ_c are the angles imposed on the front tire of the driver and controller, respectively; and the lateral slip angles of the tires are defined as follows:

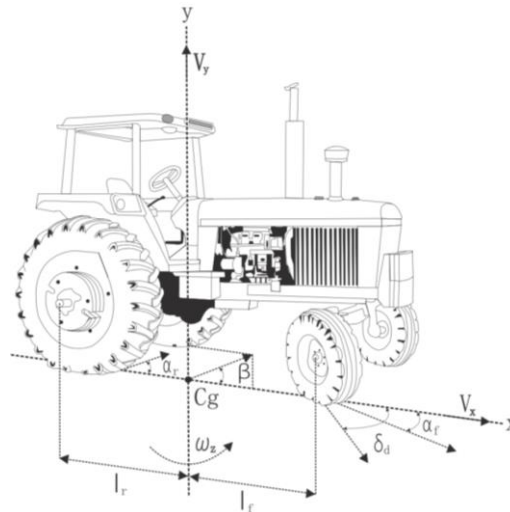


Figure 3. Bicycle model used for agricultural vehicle.

$$\alpha_f = \delta_c + \delta_d - \frac{v_y + l_r \dot{\delta}_{dact} R}{v_x} \tag{4}$$

$$\alpha_r = -\frac{v_y - l_r \omega_z}{v_x} \tag{5}$$

The control inputs δ_c and M_z are set as a state feedback problem.

2.3. Control Structure

Rewriting Equations (2) and (3), we obtain

$$\dot{v}_y = -v_x \omega_z + \frac{1}{m} (F_{f,y}(x, \delta, \alpha_f) + F_{r,y}(x, \alpha_r)) \tag{6}$$

$$\dot{\omega}_z = \left(\frac{1}{J}\right) (l_f F_{f,y}(x, \delta, \alpha_f) - l_r F_{r,y}(x, \alpha_r)) + \frac{M_z}{J} \tag{7}$$

The lateral acceleration a_y can be expressed using Newton’s second law in terms of the lateral tire forces:

$$a_y = \frac{1}{m} (F_{f,y}(x, \delta, \alpha_f) + F_{r,y}(x, \alpha_r)) \tag{8}$$

Lateral force can be defined using the well-known magic formula [30]:

$$F_{j,y} = D_{j,y} \cdot C_{j,y} \cdot B_{j,y} \cdot \alpha_j \tag{9}$$

where $j = f, r$. The constants $B_{j,y}$, $C_{j,y}$, $D_{j,y}$ in (2) and (3) are determined by Table 1.

Table 1. Actual parameters used in vehicle simulation.

$m = 4000 \text{ kg}$	$D_{r,y} = 7834$	$D_{r,yref} = 10,000 \text{ N}$
$J = 3552 \text{ kg m}^2$	$C_{r,y} = 1.32$	$C_{r,yref} = 1.38$
$l_r = 1.48 \text{ m}$	$B_{f,y} = 6.9$	$B_{f,yref} = 6.2$
$l_f = 1.30 \text{ m}$	$C_{f,y} = 1.78$	$C_{f,yref} = 1.21$
$B_{r,y} = 10$	$D_{f,y} = 7240 \text{ N}$	$D_{f,yref} = 10,000 \text{ N}$
$B_{r,yref} = 7$		

The longitudinal acceleration a_x is considered almost zero because longitudinal velocity v_x is practically constant. In addition, the front and rear lateral forces can be analyzed considering the coefficients $C_f = D_{f,y} \cdot C_{f,y} \cdot B_{f,y}$ and $C_r = D_{r,y} \cdot C_{r,y} \cdot B_{r,y}$, obtaining: $F_{f,y} = C_f \alpha_f$ and $F_{r,y} = C_r \alpha_r$.

The main aim of control is that the output system $x = [v_y, \omega_z]$ asymptotically follows a reference system $x_{ref} = [v_{y,ref}, \omega_{z,ref}]$, which it has the main characteristic of its derivatives being limited. More precisely, the reference is

$$\dot{v}_{y,ref} = -\omega_{z,ref} v_x + \frac{1}{m} (F_{fy,ref}(\delta_d, x_{ref}, \alpha_{f,ref}) + F_{ry,ref}(x_{ref}, \alpha_{r,ref})) \tag{10}$$

$$\dot{\omega}_{z,ref} = \left(\frac{1}{J_{ref}} \right) (l_f F_{fy,ref} - l_r F_{ry,ref}) \tag{11}$$

where $J_{ref} = J$, and $F_{fy,ref}, F_{ry,ref}$ are ideal curves depending on the following:

$$\alpha_{f,ref} = \delta_d - \frac{v_{y,ref} + l_f \omega_{z,ref}}{v_x} \tag{12}$$

$$\alpha_{r,ref} = -\frac{v_{y,ref} - l_r \omega_{z,ref}}{v_x} \tag{13}$$

Then, the state feedback linearization control is designed, which uses the behavior for the dynamics of lateral and turn speeds; this is done by tuning the reference signal (10) and (11) through the implementation of the control inputs δ_c and M_z .

2.4. Controller and Observer Design

Considering the Equations (6) and (7), with the front and rear lateral forces ($F_{f,y} = C_f \alpha_f$ and $F_{r,y} = C_r \alpha_r$),

$$\dot{v}_y = \left(\frac{-C_f - C_r}{m v_x} \right) v_y + \left(\frac{-C_f l_f R + C_r l_r R}{m v_x} - v_x R \right) \dot{\delta}_{dact} + \left(\frac{C_f}{m} \quad 0 \right) \begin{pmatrix} \delta \\ M_z \end{pmatrix} \tag{14}$$

$$\dot{\omega}_z = \left(\frac{-C_f l_f + C_r l_r}{J v_x} \right) v_y + \left(\frac{-C_f l_f^2 R - C_r l_r^2 R}{J v_x} \right) \dot{\delta}_{dact} + \left(\frac{C_f l_f}{J} \quad \frac{1}{J} \right) \begin{pmatrix} \delta \\ M_z \end{pmatrix} \tag{15}$$

In Equations (10) and (11), front and rear lateral forces are taken into account, with the following coefficients $C_{f,ref} = D_{f,yref} \cdot C_{f,yref} \cdot B_{f,yref}$ and $C_{r,ref} = D_{r,yref} \cdot C_{r,yref} \cdot B_{r,yref}$, obtaining $F_{fy,ref} = C_{f,ref} \alpha_{f,ref}$ and $F_{ry,ref} = C_{r,ref} \alpha_{r,ref}$, where $C_{f,ref} \neq C_f$ and $C_{r,ref} \neq C_r$. Therefore, the reference system is obtained as follows:

$$\begin{pmatrix} \dot{v}_{y,ref} \\ \dot{\omega}_{z,ref} \end{pmatrix} = \begin{pmatrix} \frac{-(C_{f,ref} + C_{r,ref})}{m v_x} & \frac{-(C_{f,ref} l_f - C_{r,ref} l_r)}{m v_x} - v_x \\ \frac{-(C_{f,ref} l_f - C_{r,ref} l_r)}{J_{ref} v_x} & \frac{-(C_{f,ref} l_f^2 + C_{r,ref} l_r^2)}{J_{ref} v_x} \end{pmatrix} \begin{pmatrix} v_{y,ref} \\ \omega_{z,ref} \end{pmatrix} + \begin{pmatrix} \frac{C_{f,ref}}{m} \\ \frac{C_{f,ref} l_f}{J_{ref}} \end{pmatrix} \delta_d \tag{16}$$

Considering errors for lateral and angular rate of turn,

$$e_{vy} = v_y - v_{y,ref} \tag{17}$$

$$e_{\omega z} = \omega_z - \omega_{z,ref} \tag{18}$$

The dynamic errors are developed by

$$\dot{e}_{vy} = \dot{v}_y - \dot{v}_{y,ref} \tag{19}$$

$$\dot{e}_{\omega z} = \dot{\omega}_z - \dot{\omega}_{z,ref} \tag{20}$$

Regarding the requirements for the control law establishing a Lyapunov function,

$$V = \frac{1}{2}e_{vy}^2 + \frac{1}{2}e_{\omega z}^2 \tag{21}$$

where (21) being positive shows that it is continuously decreasing along any path and its negative derivative, ensuring asymptotic stability as shown below

$$\begin{aligned} \dot{V} = e_{vy} & \left[\left(\frac{-C_f - C_r}{mv_x} \right) v_y + \left(\frac{-C_f l_f R + C_r l_r R}{mv_x} - v_x R \right) \dot{\delta}_{dact} + \left(\frac{C_f}{m} \right) \delta_d + \left(\frac{C_f}{m} \right) \delta_c - \dot{v}_{y,ref} \right] \\ + e_{\omega z} & \left[\left(\frac{-C_f l_f + C_r l_r}{Jv_x} \right) v_y + \left(\frac{-C_f l_f^2 R - C_r l_r^2 R}{Jv_x} \right) \dot{\delta}_{dact} + \left(\frac{C_f l_f}{J} \right) \delta_d + \left(\frac{C_f l_f}{J} \right) \delta_c + \frac{M_z}{J} - \dot{\omega}_{z,ref} \right] \end{aligned} \tag{22}$$

Furthermore, the following terms in Equation (22) are equal to gains multiplied by error, establishing the Lyapunov derivative function less than zero:

$$\left(\frac{-C_f - C_r}{mv_x} \right) v_y + \left(\frac{-C_f l_f R + C_r l_r R}{mv_x} - v_x R \right) \dot{\delta}_{dact} + \left(\frac{C_f}{m} \right) \delta_d + \left(\frac{C_f}{m} \right) \delta_c - \dot{v}_{y,ref} = -k_1 e_{vy} \tag{23}$$

$$\left(\frac{-C_f l_f + C_r l_r}{Jv_x} \right) v_y + \left(\frac{-C_f l_f^2 R - C_r l_r^2 R}{Jv_x} \right) \dot{\delta}_{dact} + \left(\frac{C_f l_f}{J} \right) \delta_d + \left(\frac{C_f l_f}{J} \right) \delta_c + \frac{M_z}{J} - \dot{\omega}_{z,ref} = -k_2 e_{\omega z} \tag{24}$$

Therefore, from Equations (23) and (24), the control inputs are acquired:

$$\delta_c = \left(\frac{1}{v_x} + \frac{C_r}{C_f v_x} \right) v_y + \left(\frac{l_f R}{v_x} - \frac{C_r l_r R}{C_f v_x} + \frac{mv_x R}{C_f} \right) \dot{\delta}_{dact} - \delta_d + \left(\frac{m}{C_f} \right) \dot{v}_{y,ref} - \left(\frac{m}{C_f} \right) k_1 e_{vy} \tag{25}$$

$$M_z = \left(\frac{C_f l_f - C_r l_r}{v_x} \right) v_y + \left(\frac{C_f l_f^2 R + C_r l_r^2 R}{v_x} \right) \dot{\delta}_{dact} - (C_f l_f) \delta_d - (C_f l_f) \delta_c + J \dot{\omega}_{z,ref} - J k_2 e_{\omega z} \tag{26}$$

where $k_i > 0$, $i = 1, 2$, and the control inputs in (25) and (26) are used in (22), verifying the stability of the system:

$$\dot{V} = -k_1 e_{vy}^2 - k_2 e_{\omega z}^2 \tag{27}$$

The Lyapunov derivative (27) can be rewritten as follows:

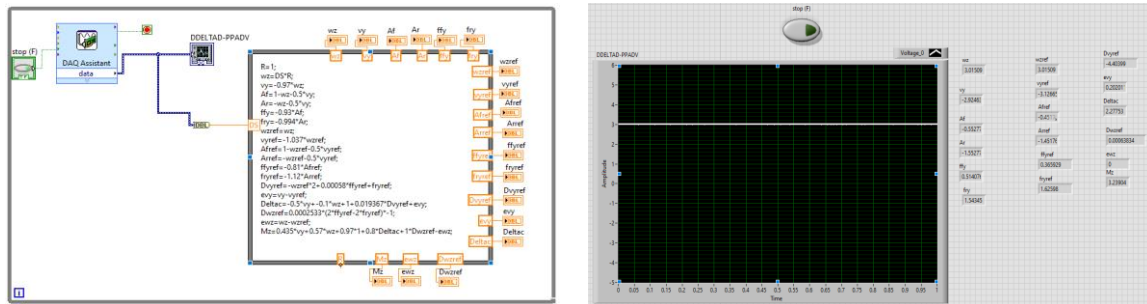
$$\dot{V} \leq -\lambda_{mink} \|e\|^2. \tag{28}$$

This establishes a $\lambda_{mink} > 0$, representing a minimum gain for k_1, k_2 with $e = (e_{vy}, e_{\omega z})$.

3. Computational Modeling for the PPTD

3.1. Model Simulations with LabVIEW and Arduino

The physical implementation can be programmed on IDE-Arduino (if a 2016 low-cost platform is desired) or a Daq 6009 NI/USB card programmed in LabVIEW software with virtual icons (at a higher cost but also applicable with the PPTD). Figure 4a illustrates the programming on LabVIEW, while Figure 4b shows the Arduino coding. Files can be downloaded at <https://drive.google.com/file/d/1bK0KADF9bKxLhTbUF6vVcYXjKpJAYhRU/view?usp=sharing> and https://drive.google.com/file/d/1i4Nsj71eZP_8_zr4KkM60x9y5QHH4Vo0/view?usp=sharing.



(a)

```
fFyref= AlfaFref*(-0.83);
fRyref= AlfaRref*(-1.13);
EWz=Wz-Wzref;
EVy=Vy-Vyref;
DerVyref= -
Wzref*Vx+(0.00058)*(fFyref+fRyref);
DeltaC=(-0.5)*Vy+(-
0.1)*Wz+constantejd+(0.019367*DerVyref)+
EVy;
```

```
void loop() {
  sensorValueA0 = analogRead(sensorA0);
  sensorValueA1 = analogRead(sensorA1);
  sensorValueA2 = analogRead(sensorA2);
  sensorValueA3 = analogRead(sensorA3);
  jd=sensorValueA0/204.8;
  Wz=jd*R;
  Vy=(Wz)*(-0.97);
  AlfaF=1 +(-lf_vx*Wz)-(Vy*0.5);
```

(b)

Figure 4. (a) Programming on IDLE-LabVIEW to obtain dynamic variables. (b) Programming on Arduino for PPTD.

The programming is designed to receive the signals δ_d and δ_c coming from the PPTD, and then the dynamics of Section 2 are analyzed either with LabVIEW or Arduino.

3.2. Design of an Operational Amplifier Circuits in Proteus Software for Physical Implementation

The hardware is made using operational amplifier circuits (TL084), as can be seen in Figure 5. This LM555 monostable circuit configuration manually simulates a 5 V amplitude step signal (high state) with a time determined by $T = 1.1 \cdot R \cdot C$, $R = R_2$, and $C = C_1$ as manual input to the platform PPTD, where the output of 5 V represents the degrees of the steering wheel on the tractor’s steering bar. The inverting op-amp in Figure 6a offers the output $-\delta_d$ and $+\delta_d$ an adjustable gain (RV1) for a single flywheel maneuver, whereas, in the electrical diagram in Figure 6b, $-\delta_d$ and $+\delta_d$ show a double steering maneuver and an amplification of the signal given by RV3 or by means of the data acquisition card 6009 or by Arduino.

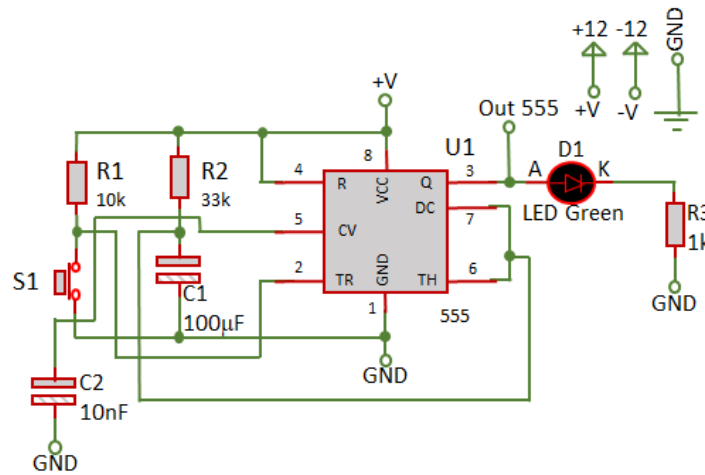


Figure 5. Circuit to obtain δ_d and manually test the PPTD.

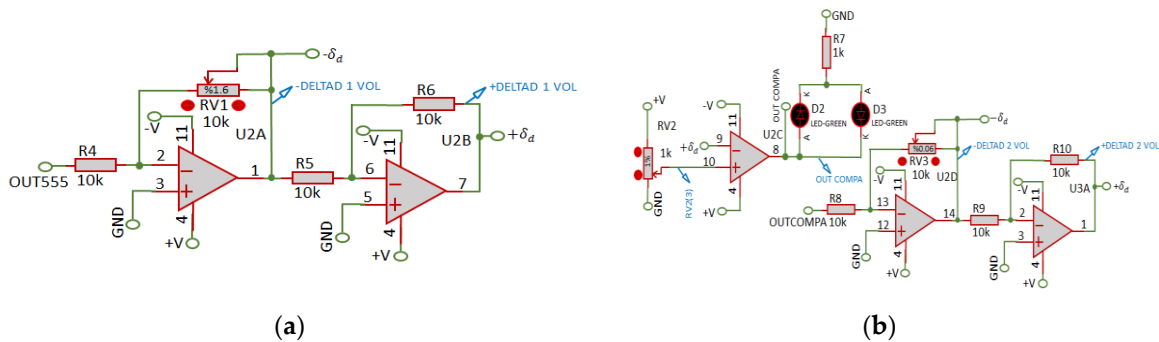


Figure 6. Circuit to generate the signal $-\delta_d, +\delta_d$ of single and double turn steering wheel in the PPTD. (a) Steering wheel angle of a single maneuver. (b) Steering wheel angle of a double maneuver.

Analyzing the uncontrolled angular and lateral velocities shown in Figure 7a, it is considered that $\omega_z \cong \dot{\delta}_{dact}R$, which is derived in Appendix A, to establish $\dot{\delta}_{dact}$, established as +DDELTA 1 VOL and DDELTA 2 VOL with an adjustable gain RV33 and RV34; in addition to R, a gain is defined by RV4/R11, resulting in the velocity signal turn $-\omega_z$ of the first op-amp (U3B), and then is multiplied by a unitary gain R13/R12 U3C generating ω_z which multiplies at the constant speed v_x represented by RV5/R14 in U3D. In order to obtain part of the algorithm for $-\dot{v}_y$ and its counterpart $-\dot{v}_y$ and R16/R15 are multiplied, generating \dot{v}_y in UA4 (Appendix B). Similarly, the reference system shown in Figure 7b is designed to analyze the reference system $-v_{y,ref}, v_{y,ref}$ to integrate $\dot{v}_{y,ref}$ (Appendix C). To obtain $\dot{\omega}_z$ and $\dot{\omega}_{z,ref}$ derive $-\omega_z$ and $-\omega_{z,ref}$ (as shown in Appendix D), where R57 and C3 are on U10B and R58 and C4 are on U10C, to set the derivative time.

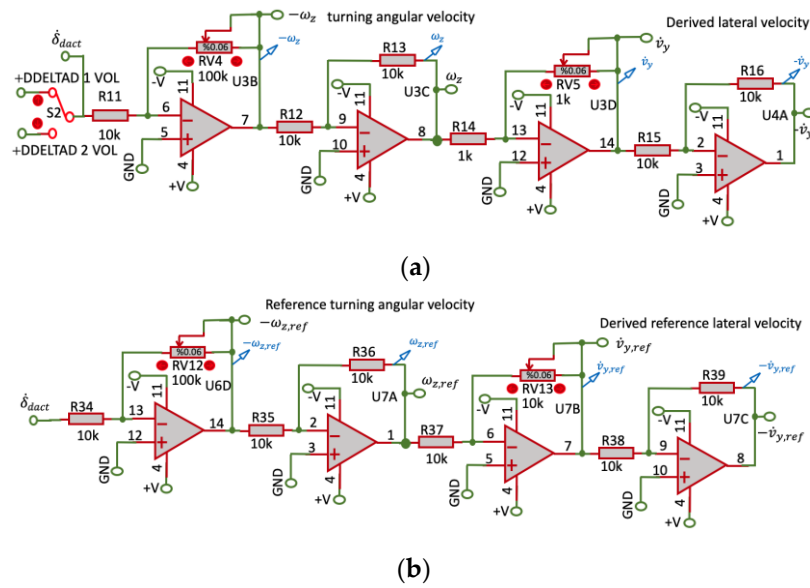


Figure 7. Circuit to generate signals in the PPTD: (a) $-\omega_z, \omega_z, \dot{v}_y = -v_x\omega_z, -\dot{v}_y = v_x\omega_z$; (b) $-\omega_{z,ref}, \omega_{z,ref}, \dot{v}_{y,ref} = -\omega_{z,ref}v_x, -\dot{v}_{y,ref} = \omega_{z,ref}v_x$. (a) Angular and lateral speeds without control. (b) Angular and lateral speeds of the reference system.

To obtain the uncontrolled frontal slip angle α_f , the input to U4B, $-v_y$ is multiplied by the gain RV6/R17, which represents $\frac{1}{v_x}$, resulting in $\frac{v_y}{v_x}$. In U4C, the exit algorithm is $\omega_z \cdot RV7/R18 (\frac{l_f}{v_x})$. Similarly, for U4D, the output is the inversion of the input δ_d multiplied by the unity gain RV8/R19, and for U5A it is an inverter summing amplifier of gain one that offers the signal $\alpha_f = \delta_d - \frac{v_y + l_f \dot{\delta}_{dact} R}{v_x}$, with the tire angle component imposed by the controller equal to zero (see Equation (4)). Figure 8b is used to analyze Equation (12).

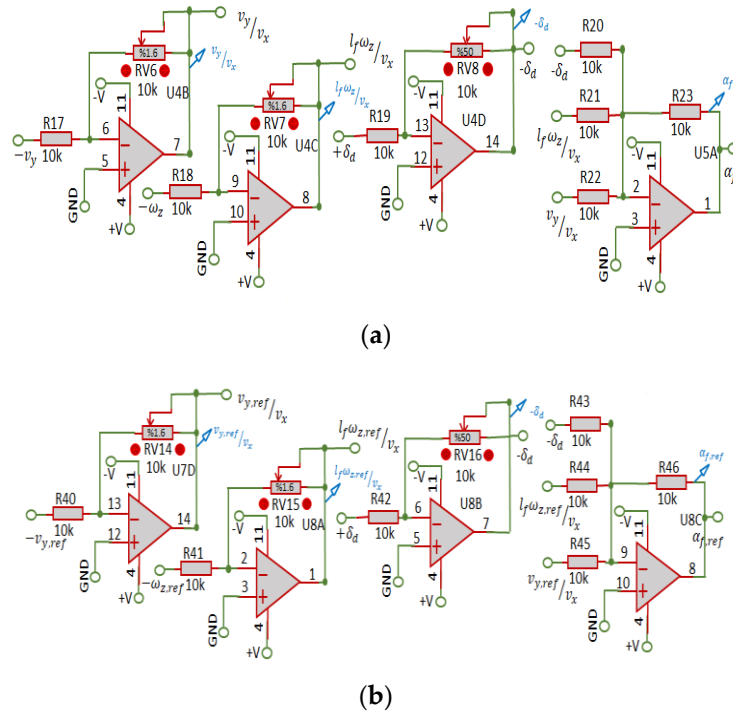


Figure 8. Signals of $\alpha_f, \alpha_{f,ref}$ in the PPTD. (a) Front sliding angle without control. (b) Front sliding angle of the reference system.

In Figure 9a, the rear slip angle α_r is shown; U5B has the input of $+\omega_z$ that multiplies the gain $RV9/R24 = \frac{l_r}{v_x}$, and remembering U4B from Figure 8a, obtains the output of $\frac{v_y}{v_x}$, which is multiplied by the unit gain $R27/R25$ of U5C and then is added to the output of U5B ($-\frac{\omega_z \cdot l_r}{v_x}$) to obtain $\alpha_r = -\frac{v_y - l_r \omega_z}{v_x}$ (see Equation (5)). Similarly, Figure 9b is used to analyze Equation (13).

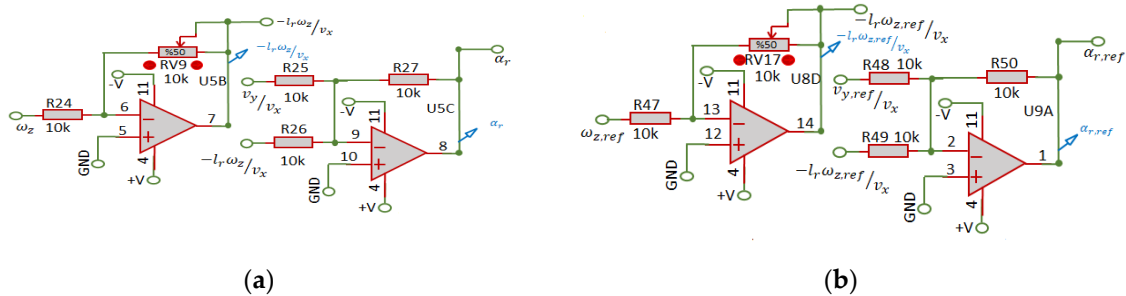


Figure 9. Signals of rear sliding angles ($\alpha_r, \alpha_{r,ref}$). (a) Rear sliding angle of the floor without control. (b) The rear sliding angle of the floor for the reference system.

In developing the front force of the tires $F_{f,y}$, in Figure 10a, U5D has the input α_f without control (the output from U5A in Figure 8a) multiplied by the gain $RV10/R28$ that simulates the coefficient C_f , so that at the output of the amplifier (U5D) $+F_{f,y}$ is obtained; then, this is multiplied by the unit gain $R30/R29$ of U6A, resulting in $-F_{f,y}$ of the Equation (9). The same criteria are used in Figure 10b for the reference signals.

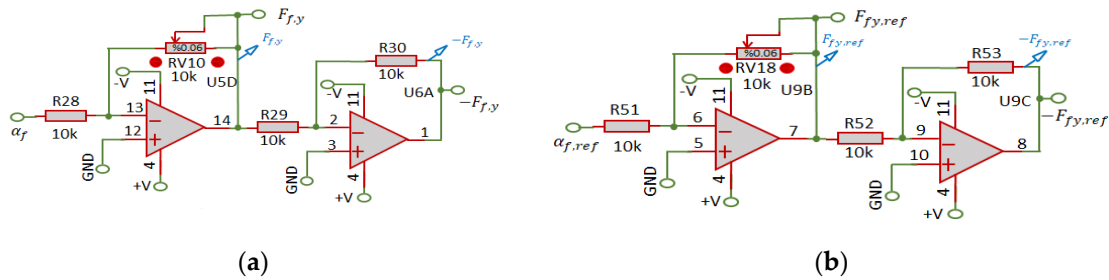


Figure 10. Obtention of front signals $-F_{f,y}, F_{f,y}, -F_{f,y,ref}, F_{f,y,ref}$ in PPTD. (a) Uncontrolled front force. (b) Front reference force.

In Figure 11a, $RV19/R54$ gain is named as the coefficient C_r that multiplies at the input of the amplifier α_r , acquiring $F_{r,y}$, which multiplies a unit gain of $R33/R32$ to have an output of U6C at $-F_{r,y}$, studied in Equation (9). Analogously, Figure 11b is proposed.

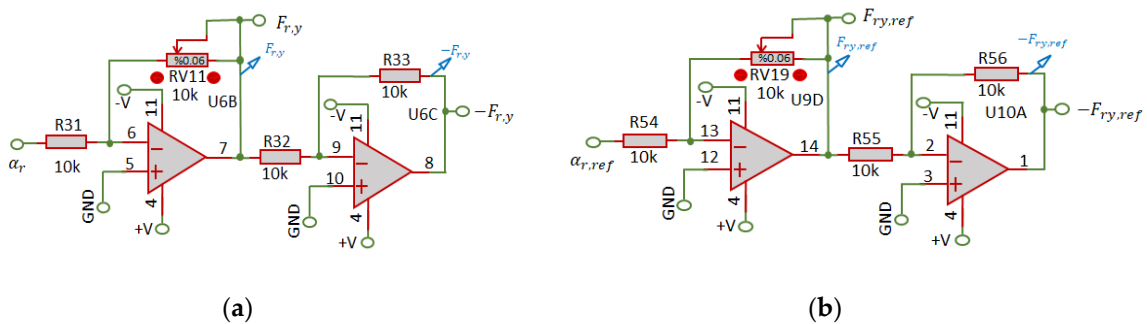


Figure 11. Obtention of front signals $F_{r,y}, F_{r,y,ref}$ in PPTD. (a) Uncontrolled rear force. (b) Rear force for the reference system.

Only one summing inverting amplifier is appended to consider the front forces $-F_{f,y}, -F_{f,y,ref}$ and rear forces $F_{r,y}, F_{r,y,ref}, -F_{r,y}, -F_{r,y,ref}$ for the installed system, and another is used for the reference

system in Figure 7, obtaining two new circuits that complete Equations (2), (3), (10), and (11) without control inputs.

In terms of errors (Appendix E), for e_{vy} (Equation (17)), a subtraction amplifier is used with the inputs of v_y versus $v_{y,ref}$; for $e_{\omega z}$, it has the subtraction of ω_z minus $\omega_{z,ref}$ employing an operational amplifier in subtractor mode (see Equation (18)).

When analyzing the system installed on the agricultural vehicle and the local reference system, it is possible to establish the controller design. Starting with the control input δ_c (Figure 12), the gain $G1 = RV20/R67$ which represents the value $\frac{1}{v_x} + \frac{C_r}{C_f v_x}$ is defined; this multiplies the input of the lateral velocity v_y to obtain the output of U11B, representing the algorithm for $-\left(\frac{1}{v_x} + \frac{C_r}{C_f v_x}\right) \cdot v_y$. Furthermore, for the controlled turning angular velocity, $\omega_z \cong \dot{\delta}_{dact}R$ is multiplied by $RV21/R68 = G2 = \frac{l_f}{v_x} - \frac{C_r l_r}{C_f v_x} + \frac{m v_x}{C_f}$, obtaining the output U11C, $-\left(\frac{l_f}{v_x} - \frac{C_r l_r}{C_f v_x} + \frac{m v_x}{C_f}\right) \cdot \dot{\delta}_{dact}R$.

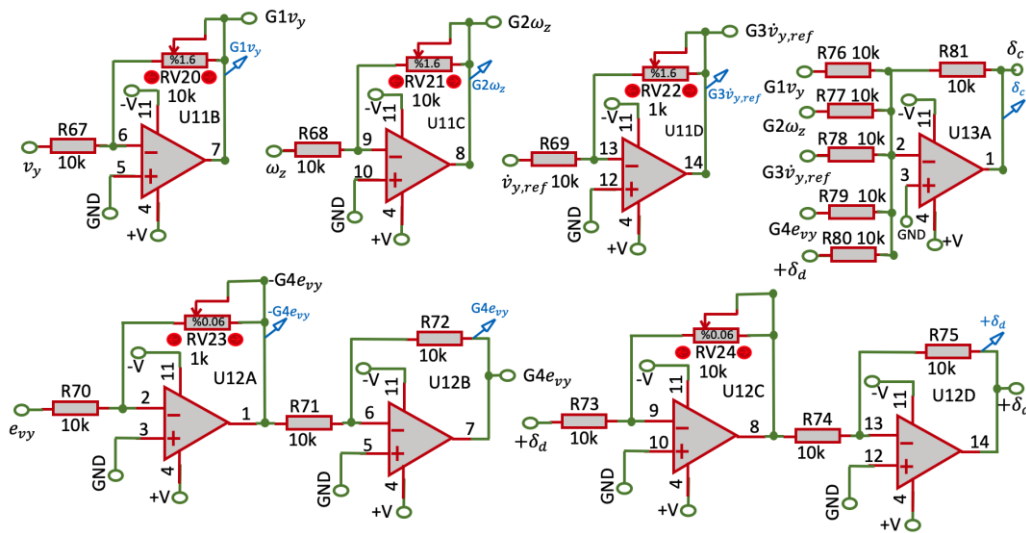


Figure 12. Control entry of δ_c to the PPTD.

$\dot{v}_{y,ref}$, as input for U11D, is multiplied by the gain $RV22/R69 = G3 = \frac{m}{C_f}$, which results in the output of the same amplifier (U11D), $-\frac{m}{C_f} \cdot \dot{v}_{y,ref}$.

The lateral velocity error e_{vy} is multiplied by a gain of $RV23/R70 = -G4 = -k_1 \cdot \frac{m}{C_f}$, obtaining U12A $= -\frac{m}{C_f} \cdot k_1 \cdot e_{vy}$ at the output of U12B with unity gain of $R72/R71 = +G4$ and with input $-\frac{m}{C_f} \cdot k_1 \cdot e_{vy}$ resulting in $\frac{m}{C_f} \cdot k_1 \cdot e_{vy}$.

In U13A, a unit gain inverting adder is applied with the inputs $-\left(\frac{1}{v_x} + \frac{C_r}{C_f v_x}\right) \cdot v_y - \left(\frac{l_f}{v_x} - \frac{C_r l_r}{C_f v_x} + \frac{m v_x}{C_f}\right) \cdot \dot{\delta}_{dact}R - \frac{m}{C_f} \cdot \dot{v}_{y,ref} + \frac{m}{C_f} \cdot k_1 \cdot e_{vy} + \delta_d$ (integrated), and at the output (U41), $\delta_c = \left(\frac{1}{v_x} + \frac{C_r}{C_f v_x}\right) v_y + \left(\frac{l_f R}{v_x} - \frac{C_r l_r R}{C_f v_x} + \frac{m v_x R}{C_f}\right) \dot{\delta}_{dact} - \delta_d + \left(\frac{m}{C_f}\right) \dot{v}_{y,ref} - \left(\frac{m}{C_f}\right) k_1 e_{vy}$, as proposed in Equation (25).

Following the control inputs, a controller is also proposed for the agricultural vehicle, when there is a dynamic and nonfixed rear axle, as an innovative idea for M_z , seen in Figure 13 and Equation (26). In U13B, the input v_y multiplies the gain $RV25/R82 = M1 = \frac{C_f l_f - C_r l_r}{v_x}$, obtaining the output $-\left(\frac{C_f l_f - C_r l_r}{v_x}\right) \cdot v_y$. For U13C, $\omega_z \cong \dot{\delta}_{dact}R$ multiply the gain $M2 = RV26/R83 = \frac{C_f l_f^2 + C_r l_r^2}{v_x}$, obtaining the output $-\left(\frac{C_f l_f^2 + C_r l_r^2}{v_x}\right) \cdot \dot{\delta}_{dact}R$.

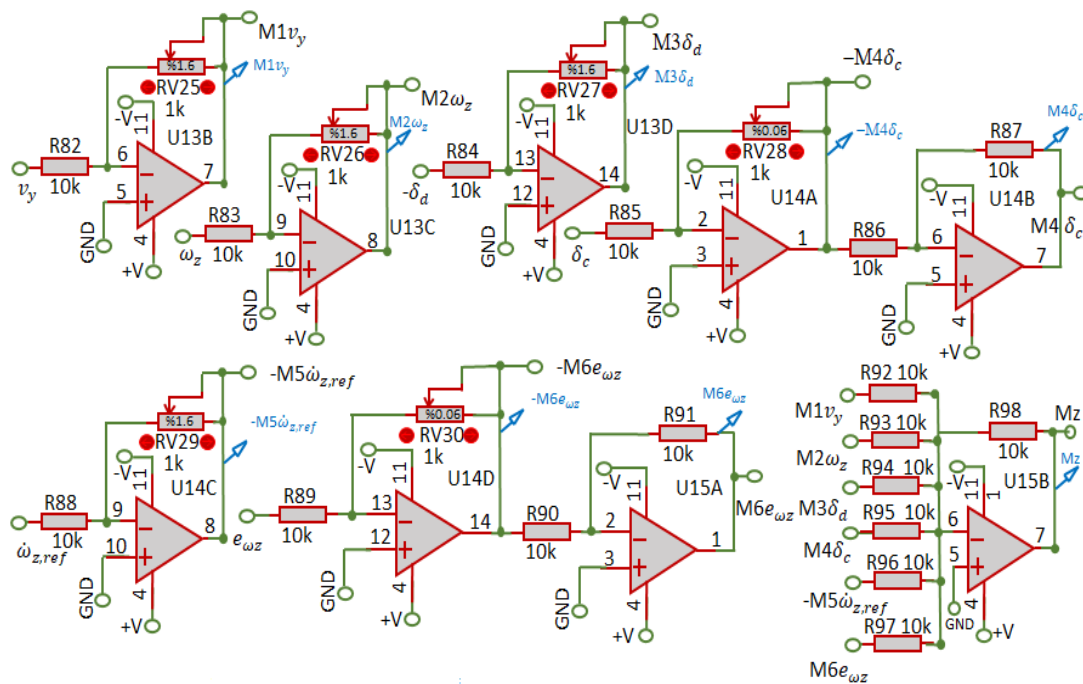


Figure 13. Control entry of M_z PPTD.

In U13D, the input $-\delta_d$ is multiplied by $RV27/R84 = M3 = C_f l_f$, resulting in $C_f l_f \delta_d$. In U14A, the input δ_c is multiplied by $RV28/R85 = C_f l_f = -M4$, obtaining the output $-C_f l_f \delta_c$ that multiplies U14B by $R87/R86$ (unity gain) and thus obtains the output $C_f l_f \delta_c$. Similarly, for U14C, the input $\omega_{z,ref}$ multiplies the gain $RV29/R88 = M5 = -J$, resulting in $-J\omega_{z,ref}$.

In U14D, it is considered that input $e_{\omega z}$ multiplies the gain $RV30/R89 = -M6$, resulting in $-J \cdot k_2 \cdot e_{\omega z}$. This is multiplied by U15A and the unit gain $R91/R90$ to obtain the output $J \cdot k_2 \cdot e_{\omega z}$. With this, there is an inverting adder in U15B that has as inputs $-\left(\frac{C_f l_f - C_r l_r}{v_x}\right) \cdot v_y$, $-\left(\frac{C_f l_f^2 + C_r l_r^2}{v_x}\right) \cdot \delta_{dact} R$, $C_f l_f \delta_d$, $C_f l_f \delta_c$, $-J \cdot \omega_{z,ref}$, and $J \cdot k_2 \cdot e_{\omega z}$. Therefore, Equation (26) is obtained.

The circuit of Appendix F receives the signal from the actuators a (δ) and b (δ) and conditions it for input to the PPDT. All of these Proteus files schemes (Figures 5–13) can be downloaded at https://drive.google.com/drive/folders/1_Y9uqd5n78ZJP-8v-zt8Tbjqa2wfow5I?usp=sharing.

4. Hardware Implementation

4.1. Design of Circuit Board

After having tested the programming logic on the Arduino card and on the DAQ 6009 NI/USB, the 3D view circuit in Figure 14 was designed with the support of the Layout function on Proteus Software (https://drive.google.com/drive/folders/1bvDvBBjuuHQ6LBpOLXgntjFL51V3_vSx?usp=sharing). It can be manufactured by the SMT method, and another alternative may be made with a PCB-type board. As can be seen, the PPTD is an extremely compact manufactured device. The circuit board was connected to an APP, also shown in Figure 14, through Bluetooth. The APP was built in APP-inventor with the aim of observing the main parameters in real time while the tractor is operated autonomously with a set time interval determined every 5 s. Table 2 summarizes the main device characteristics and their costs.

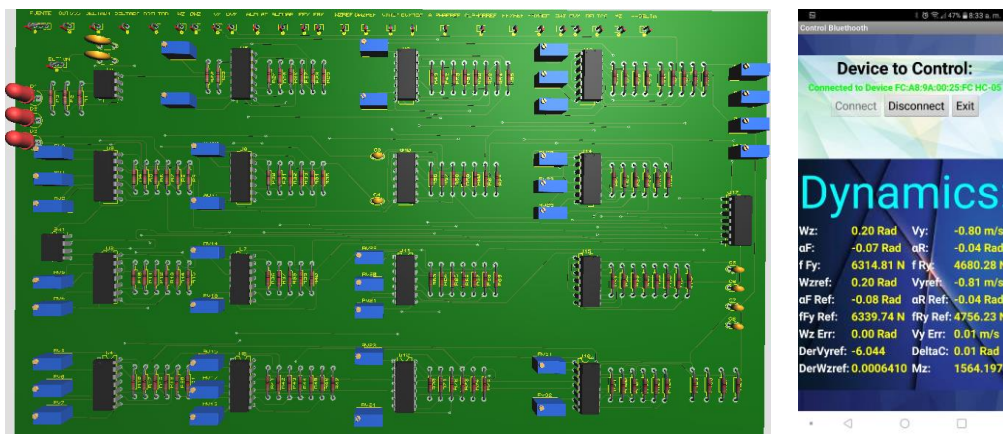


Figure 14. 3D view of the implemented circuit (PPTD).

Table 2. Main characteristics of the PPTD (currency: USD).

Quantity	Device	Cost	Total Cost
1	LM555	0.25	0.25
16	TL084	0.34	5.44
3	Led	0.0425	0.12
1	Switch push-button	0.431	0.431
30	Pines	0.025	0.75
1	Capacitor 10 nF	0.0645	0.645
5	Capacitor 100 μ F/25 V	0.086	0.43
2	Capacitor 0.1 μ F/25 V	0.0645	0.129
2	Potentiometer 100 k Ω	0.3665	0.733
4	Potentiometer 50 k Ω	0.3665	1.466
20	Potentiometer 10 k Ω	0.3665	7.33
10	Potentiometer 1 k Ω	0.3665	3.665
1	Resistance 33 k Ω Potentiometer 10 Ω Resistance 33 k Ω	0.0215	0.0215
104	Resistance 10 k Ω	0.0215	2.36
3	Resistance 1 k Ω	0.0215	0.0645
16	Base for integration	0.1	1.6
1	PCB PPTD	25	25
Total			50.98

4.2. Experimental Setup Applied on a Real Tractor

The experimental part of the PPTD platform was implemented in the fields of crops as a real application. The connections and programming were established for the analysis of the dynamics of an agricultural vehicle. An electric motor was adapted as an actuator on the steering wheel of the tractor, as shown in Figure 15. The PPTD platform connection on the agricultural vehicle continued to obtain the measurements of the tractor dynamics variables in real time. Afterward, those variables were compared with the simulations done with the modeling equations representing the tractor. Some videos of the routes that were carried out with measurements and autonomy control are shown in the following link: <https://drive.google.com/drive/folders/1Tpc9ZQ0Ncm5Dbwi6LXHMjZy46irBJuoG?usp=sharing>.

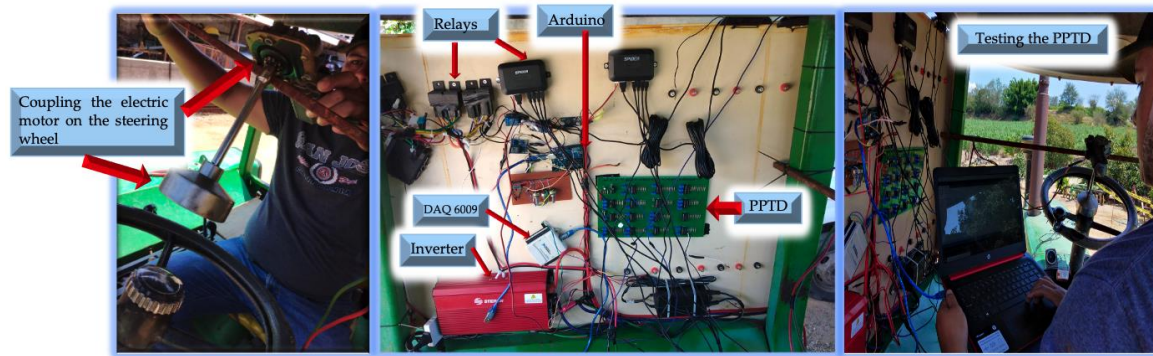


Figure 15. Mechanical implementation of the steering wheel with the CC motor for autonomy control.

5. Results and Discussion

The results of the dynamics and variables for the PPTD coupled to the DAQ-6009 and Arduino were compared with the dynamics model schematics using MATLAB-Simulink [37]. Figures 16 and 17 represent a turn change in the tractor steering wheel to analyze its response and analyze the response of the algorithm and tool better. Figure 16 illustrates the response of the angular velocity on the platform with Arduino, with LabView, and with the simulations made in MATLAB, where the platform found the reference faster than the simulations. In the simulations, a PID control algorithm implemented the Ziegler–Nichols method with a $k_p = 0.1$ and $k_i = 0.00218$ and a derivative gain $k_d = 0.00007$, while the platform control algorithm was implemented as presented in Section 2.4. Figure 17 illustrates the lateral velocity, which is the other control signal presented in Section 2.4, the response of which was similar to that of ω_z in that the platform reached the reference faster than the simulations. This is due to the input of the sensor for signal V_y in Arduino: a pulse signal is programmed in Arduino so that the response of the speed estimate is given in milliseconds and accelerates the response of the control to the output. The graphs illustrate a satisfactory response of the platform together with the proposed control algorithm; when compared to a PID, it illustrates a better control response to a change in the steering wheel of the tractor. The platform is presented in great detail from its mathematical basis to its implementation so that it can be replicated and used to analyze more complex control algorithms.

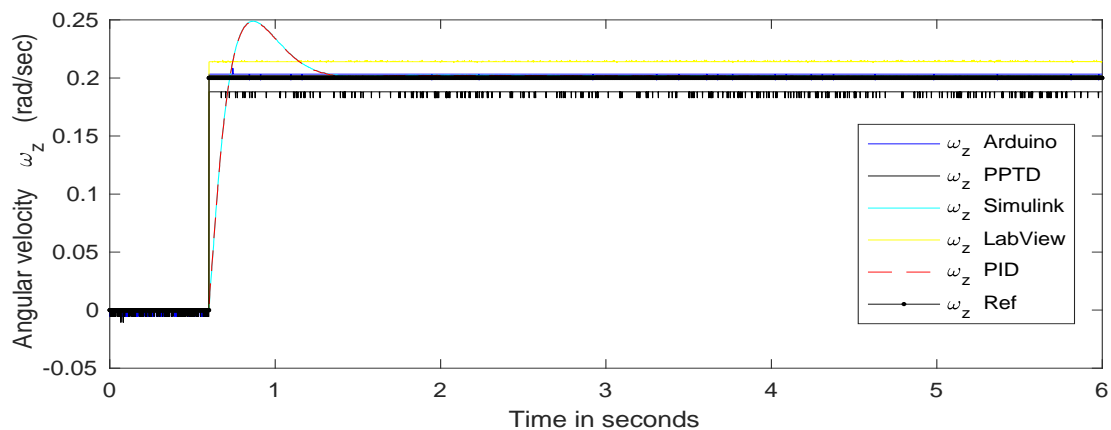


Figure 16. Estimating angular velocity ω_z .

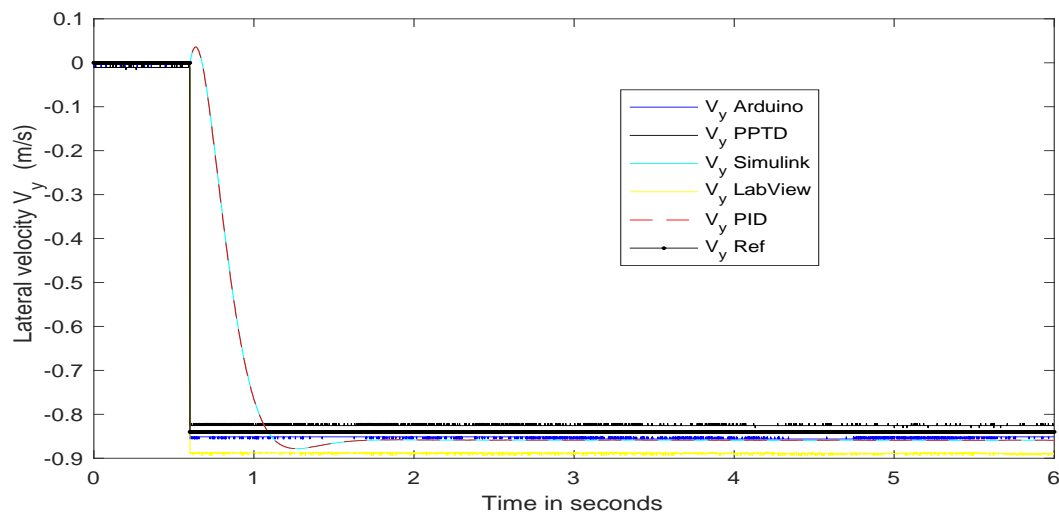


Figure 17. Estimating lateral velocity v_y .

Some suggestions to improve this proposal would be the inclusion of a more complex model of the tractor that considers other dynamics, such as drag; the implementation of other nonlinear control strategies that help to reduce the control responses in the dynamics; or the inclusion of other types of sensors, such as cameras or GPS, which would help increase the level of autonomy of the vehicle.

6. Conclusions

The low-cost platform created on operational amplifiers was proposed to comprehend the dynamics and variables of a tractor to achieve autonomy and analyze the performance of the suggested control strategy algorithms in real time by status feedback. The proposed electronic platform uses commercial sensors and interfaces with the National Instruments Daq 6009 and Arduino Uno board. Additionally, it was installed on a tractor to gain autonomy, and its operation was physically analyzed in an agricultural field due to easy installation design. It is also worth mentioning that this work presented the mathematical, control, and applicative foundation for the needs that currently arise in understanding the principles of vehicular autonomy. The presented work can also be implemented in engine system electronics for future electric tractor designs. The results obtained were compared with the models established in MATLAB found in the literature as validation of the platform, showing satisfactory results for the analysis of the dynamics of the tractor. All simulations and developments are shared via a web link as open-source files so that anyone with basic knowledge of electronics and vehicle modeling can reproduce the proposed platform.

Author Contributions: S.S.P., investigation planning, methodology, and validation; J.M.G.L., formal analysis, methodology, and writing—original draft; R.O.J.B., conceptualization and visualization; E.V.L., writing—review and editing; J.E.M.S., resources; M.G.S.C., software simulations; V.J.O.G., resources and supervision. All authors have read and agreed to the published version of the manuscript.

Funding: This research received no external funding.

Conflicts of Interest: The authors declare no conflict of interest.

Abbreviations

m	Vehicle mass [kg]
J	Moment of inertia [$\text{kg } m^2$]
l_f, l_r	Lengths from the center to the front and rear, respectively [m]
v_x, v_y	Longitudinal and lateral velocity [m/s]
β	Chassis side slide [rad]
ω_z	Angular velocity of turn [rad/s]
δ_d	Angle imposed on the front tire by driver [rad]
$\dot{\delta}_{dact}$	Angular velocity response of the actuator [rad/s]
δ_c	Angle on the front tire of the controller [rad]
δ	Function of the angle imposed on the front tires ($\delta = \delta_d + \delta_c$) [rad]
M_z	Moment of turn resulting from the active brakes [Nm]
$F_{f,y}, F_{r,y}$	Lateral front and rear forces [N]
α_f	Front side slip angles [rad]
α_r	Rear side slip angles [rad]
u_m	Input voltage to actuator [V]
R_m	Resistance of the actuator [Ω]
k_b	Back electromotive force constant (back-EMF constant) [V/(rad/s)]
M_z	Moment of turn resulting from the active brakes [Nm]
a_y	Lateral acceleration [m/s^2]
a_x	Longitudinal acceleration [m/s^2]
$v_{y,ref}$	Reference lateral velocity [m/s]
$\omega_{z,ref}$	Reference angular yaw velocity [rad/s]
$F_{fy,ref}, F_{ry,ref}$	Lateral and rear reference force [N]
$\alpha_{f,ref}, \alpha_{r,ref}$	Reference front and rear side slip angles [rad]
J_{ref}	Reference moment of inertia [$\text{kg } m^2$]

Appendix A

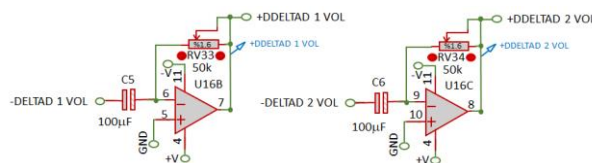


Figure A1. Angular velocity response of the actuator.

Appendix B

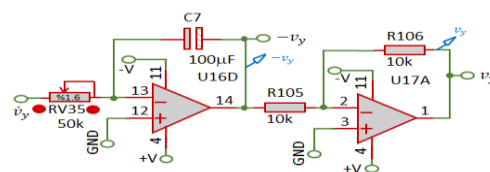


Figure A2. Lateral velocity.

Appendix C

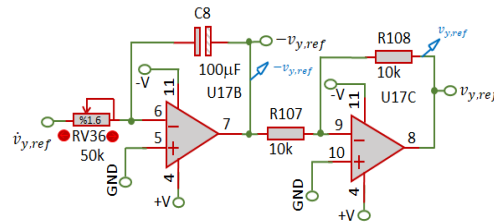


Figure A3. Reference lateral velocity.

Appendix D

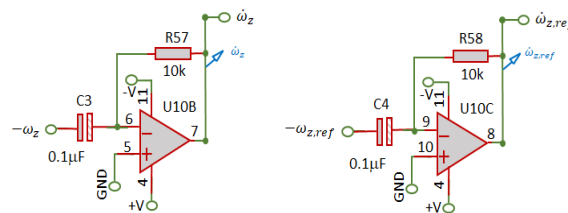


Figure A4. Reference angular yaw velocity.

Appendix E

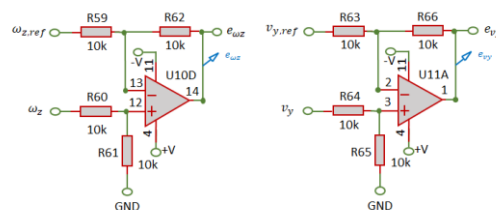


Figure A5. Errors for e_{vy} .

Appendix F

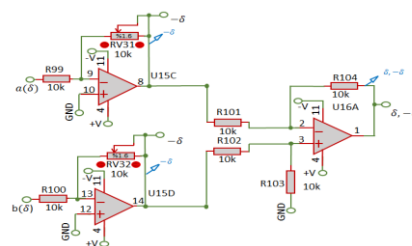


Figure A6. Function of the angle imposed on the front tires.

References

1. Lenzo, B.; Zanchetta, M.; Sorniotti, A.; Gruber, P.; de Nijs, W. Yaw Rate and Sideslip Angle Control through Single Input Single Output Direct Yaw Moment Control. *IEEE Trans. Control Syst. Technol.* **2020**. [CrossRef]
2. Acosta-Lúa, C.; di Gennaro, S.; Sánchez-Morales, M.U. An Adaptive Controller Applied to an Anti-lock Braking System Laboratory. *DYNA J. Eng.* **2016**, *83*, 69–77. [CrossRef]
3. Mansour, A.; Amir, K.; Soo, J. Model Predictive Control for integrated lateral stability, traction/braking control; rollover prevention of electric vehicles. *Veh. Syst. Dyn.* **2019**. [CrossRef]
4. Hongzhou, H.; Zhihua, Z. Explicit-Implicit Co-Simulation Techniques for Dynamic Responses of a Passenger Car on Arbitrary Road Surfaces. *Engineering* **2019**, *5*, 1171–1178.

5. Liqin, S.; Yong, L.; Guoqing, G.; Zhongxing, L.; Haobin, J. Research on Switching Interconnection Modes and Game Control of Interconnected Air Suspension. *Energies* **2019**, *12*, 1–23.
6. Fen, L.; Kaizheng, W.; Youqun, Z.; Shaobo, W. Integrated Avoid Collision Control of Autonomous Vehicle Based on Trajectory Re-Planning and V2V Information Interaction. *Sensors* **2020**, *20*, 1079.
7. Reina, G.; Milella, A.; Rouveure, R.; Nielsen, M.; Worst, R.; Blas, M.R. Ambient awareness for agricultural robotic vehicles. Special Issue: Robotic Agriculture. *Biosyst. Eng.* **2015**, *146*, 114–132. [[CrossRef](#)]
8. Cavallone, P.; Botta, A.; Carbonari, L.; Visconte, C.; Quaglia, G. The Agri. q Mobile Robot: Preliminary Experimental Tests. In Proceedings of the International Conference of IFToMM Italy, 9–11 September 2020; pp. 524–532, (online conference).
9. Cook, J.T.; Ray, L.E.; Lever, J.H. Dynamics modeling and robotic-assist, leader-follower control of tractor convoys. *J. Terramech.* **2017**, *75*, 57–72. [[CrossRef](#)]
10. Eaton, R.; Katupitiya, J.; Siew, K.W.; Howarth, B. Autonomous Farming: Modeling and Control of Agricultural Machinery in a Unified Framework. In Proceedings of the 15 International conference on Mechatronics and Machine Vision in Practice (M2VIP08), Auckland, New Zealand, 2–4 December 2008; pp. 499–504.
11. Nebot, E. Robotics: From Automation to Intelligent Systems. *Engineering* **2018**, *4*, 446–448. [[CrossRef](#)]
12. Van Loon, J.; Woltering, L.; Krupnik, T.J.; Baudron, F.; Boa, M.; Govaerts, B. Scaling agricultural mechanization services in smallholder farming systems: Case studies from sub Saharan Africa, South Asia; Latin America. *Agric. Syst.* **2020**, *180*, 1–13. [[CrossRef](#)]
13. Jia, C.; Qiao, W.; Qu, L. Modeling and Control of Hybrid Electric Vehicles: A case Study for Agricultural Tractors. In Proceedings of the Conference: 2018 IEEE Vehicle Power and Propulsion Conference (VPPC), Chicago, IL, USA, 27–30 August 2018; pp. 1–6. [[CrossRef](#)]
14. Zang, Y.; Zhu, Z.; Song, Z.; Mao, E. Virtual Reality and the Application in Virtual Experiment for Agricultural Equipment. In Proceedings of the 4th Conference on Computer and Computing Technologies in Agriculture (CCTA), Nanchang, China, 10 October 2010; pp. 257–268.
15. Kayacan, E.; Kayacan, E.; Herman, R.; Saeys, W. Modeling and Identification of the Yaw Dynamics of an Autonomous Tractor. In Proceedings of the IEEE 2013 9th Asian Control Conference (ASCC), Istanbul, Turkey, 23–26 June 2013; pp. 1–6. [[CrossRef](#)]
16. Kim, Y.-Y.; Kim, B.; Shin, S.-Y.; Kim, J.; Yum, S. Development of Driving Simulator for Safety Training of Agricultural Tractor Operators. *J. Biosyst. Eng.* **2014**, *39*, 389–399. [[CrossRef](#)]
17. Ochoa-Lleras, N.; Brennan, S.; Murphy, D.; Klena, M.J.; Garvey, H.J.; Sommer, H.J., III. Development of an Open-Source Tractor Driving Simulator for Tractor Stability Test. *J. Agric. Saf. Health* **2016**, *22*, 227–246. [[PubMed](#)]
18. Sun, C.; Nakashima, H.; Shimizu, H.; Miyasaka, J.; Ohdoi, K. Physics engine application to overturning dynamics analysis on banks and uniform slopes for an agricultural tractor with a rollover protective structure. *Biosyst. Eng.* **2018**, *185*, 150–160. [[CrossRef](#)]
19. Arena, F.; Pau, G.; Collotta, M. A survey on driverless vehicles: From their diffusion to security. *J. Internet Serv. Inf. Secur.* **2018**, *8*, 1–19.
20. Arena, F.; Ticali, D. The development of autonomous driving vehicles in tomorrow's smart cities mobility. In Proceedings of the AIP Conference International Conference of Computational Methods in Sciences and Engineering, Thessaloniki, Greece, 14–18 March 2018; Volume 2040.
21. Kuutti, S.; Bowden, R.; Jin, Y.; Barber, P.; Fallah, S. A survey of deep learning applications to autonomous vehicle control. *IEEE Trans. Intell. Transp. Syst. preprint* **2020**, 1–22. [[CrossRef](#)]
22. Fan, X.; Sun, Y. The application of ADAMS/CAR in vehicle engineering teaching. *Int. J. Contin. Eng. Educ. Life Long Learn.* **2018**, *28*, 37–53. [[CrossRef](#)]
23. Alipour, K.; Babaei-Robat, A.; Tarvirdizadeh, B. Dynamics modeling and sliding mode control of tractor-trailer wheeled mobile robots subject to wheels slip. *Mech. Mach. Theory* **2019**, *138*, 16–37. [[CrossRef](#)]
24. Vidal Bravo, S.; de la Cruz-Soto, J.; Arrieta Paternina, M. Light electric vehicle powertrain: Modeling, simulation; experimentation for engineering students using PSIM. *Comput. Appl. Eng. Educ.* **2020**, *28*, 406–419. [[CrossRef](#)]
25. De Lorenzo, Autotronica. Available online: <https://www.delorenzoglobal.com/es/autotronica/> (accessed on 12 July 2020).
26. National Instruments, Plataforma Hil. Available online: <https://www.ni.com/es-mx/innovations/automotive/hardware-in-the-loop.html> (accessed on 12 July 2020).

27. Trimble. Available online: <https://agriculture.trimble.com/product/ez-guide-250/> (accessed on 13 July 2020).
28. John Deere, Future of Farming. Available online: <https://www.deere.co.uk/en/agriculture/future-of-farming/> (accessed on 13 July 2020).
29. Bogusevschi, D.; Muntean, C.; Muntean, G.M. Teaching and Learning Physics using 3D Virtual Learning Environment: A Case Study of Combined Virtual Reality and Virtual Laboratory in Secondary School. *J. Comput. Math. Sci. Teach.* **2020**, *39*, 5–18.
30. Murray-Tortarolo, G.N.; Jaramillo, V.J.; Larsen, J. Food security and climate change: The case of rainfed maize production in Mexico. *Agric. For. Meteorol.* **2018**, *253*, 124–131. [[CrossRef](#)]
31. Shamah-Levy, T.; Mundo-Rosas, V.; Flores-De la Vega, M.; Luiselli-Fernández, C. Food security governance in Mexico: How can it be improved? *Glob. Food Secur.* **2017**, *14*, 73–78. [[CrossRef](#)]
32. Pacejka, H.B. *Tyre and Vehicle Dynamics*; Elsevier: Amsterdam, The Netherlands, 2005.
33. Rajamani, R. *Vehicle Dynamics and Control*; Springer Science and Business Media: Berlin/Heidelberg, Germany, 2011.
34. Benton-Derrick, J.; Bevely, D.M. Adaptive Control of a Farm Tractor with Varying Yaw Dynamics Accounting for Actuator Dynamics and Saturations. In Proceedings of the 17th IEEE International Conference on Control Applications Part of 2008 IEEE Multi-Conference on Systems and Control, San Antonio, TX, USA, 3–5 September 2008; pp. 547–552. [[CrossRef](#)]
35. Borri, A.; Bianchi, D.; di Benedetto, M.D.; di Gennaro, S. Optimal Workload Actuator Balancing and Dynamic Reference Generation in Active Vehicle Control. *J. Frankl. Inst.* **2017**, *4*, 1722–1740. [[CrossRef](#)]
36. Coballes-Pantoja, J.; Gómez-Fuentes, R.; Noriega, J.R.; García-Delgado, L.A. Parallel Loop Control for Torque and Angular Velocity of BLDC Motors with DTC Commutation. *Electronics* **2020**, *9*, 279. [[CrossRef](#)]
37. Zhang, H.; Heng, B.; Zhao, W. Path Tracking Control for Active Rear Steering Vehicles Considering Driver Steering Characteristics. *IEEE Access* **2020**, *8*, 98009–98017. [[CrossRef](#)]

Publisher's Note: MDPI stays neutral with regard to jurisdictional claims in published maps and institutional affiliations.



© 2020 by the authors. Licensee MDPI, Basel, Switzerland. This article is an open access article distributed under the terms and conditions of the Creative Commons Attribution (CC BY) license (<http://creativecommons.org/licenses/by/4.0/>).